Electronic Supplementary Information (ESI)

Activatable BODIPY-Chromene NIR-II probes with small spectral crosstalk endow high-contrast in vivo bioimaging

Liao Zhang, Chenxu Yan, Yutao Zhang, Dun Ma, Jialiang Huang, Zijun Zhao, Yining Tao, Caiqi Liu, Juan Li and Zhiqian Guo*

Key Laboratory for Advanced Materials and Joint International Research Laboratory of Precision Chemistry and Molecular Engineering, Feringa Nobel Prize Scientist Joint Research Center, Institute of Fine Chemicals, School of Chemistry and Molecular Engineering, East China University of Science & Technology, Shanghai 200237 (China), E-mail addresses: guozq@ecust.edu.cn

Table of Contents

General experimental details

Materials and General Methods

Unless special stated, all solvents and chemicals were purchased from commercial suppliers in analytical grade and used without further purification. The ^{1}H and ^{13}C NMR spectra were recorded on a Bruker AM 400 spectrometer, using TMS as an internal standard. High resolution mass spectrometry data were obtained with a Waters LCT Premier XE spectrometer. Absorption spectra were collected on a Varian Cary 500 spectrophotometer. Fluorescence spectra measurements were performed on a PTI-QM4 steady-stead fluorimeter with an InGaAs photodetector. Particle size was measured by dynamic light scattering (DLS) with a Malvern Zetasizer Nano S90. In vivo NIR-II fluorescence images were measured with NIR-II in vivo imaging system MARS (Artemis intelligent imaging, China).

Calculations of fluorescence quantum yield

Optical matching solutions of IR26 (Φ_{fl} = 0.05% in dichloroethane) was used as the standard to measure fluorescence quantum yield. The calculation equation is as follows:

$$\Phi_s = \Phi_r(A_rF_s/A_sF_r)(n_s^2/n_r^2)$$

r and s represent reference and sample, respectively. *n* is the refractive index of the solvent, *F* is relative integrated fluorescence intensity and *A* is the absorbance.

Determination of pKa value

The p*K*a value of BC-OH was determined using the Henderson-Hasselbalch equation:

$$Log[(A_{max}-A)/(A-A_{min})]= pKa-pH$$

Where, A represents the observed absorbance at the measured wavelength, A_{max} and A_{min} represent the maximum and minimal absorbance, respectively.

Quantum chemical calculation details

The density functional theory (DFT) and time-department DFT (TD-DFT) calculations were employed to understand the structural and electronic properties of these dyes using Gaussian 09. Geometries of these dyes were optimized at B3LYP/6-311g (d,p) basis sets. We confirmed that we obtained stable structures via frequency analysis. The vertical excitation properties were investigated at CAM-B3LYP/6-311g (d,p) level.

Preparation of BC-H_2O_2-loaded nanoparticles

BC-H_2O_2-loaded nanomicelle was prepared through a typical procedure: 2 mg BC-H_2O_2 and 9 mg DSPE-PEG2000 was added to DMSO (1 mL) and stirred for 10 min at 25 ^{o}C. Subsenquently, this mixture was dropped into the deionized

water and stirred for another 20 min. Then, dialysis was performed with deionized water for 24 h (molecular weight cutoff = 2000 g mol^{-1}). The deionized water was exchanged for 5 times.

In vitro cytotoxicity assay

The cell lines were purchased from the Institute of Cell Biology (Shanghai, China). Cells were all propagated in T-75 flasks cultured at 37 ℃ under a humidified 5% CO_2 atmosphere in RPMI-1640 medium or DMEM medium (GIBCO/Invitrogen, Camarillo, CA, USA), which were supplemented with 10 % fetal bovine serum (FBS, Biological Industry, Kibbutz Beit Haemek, Israel) and 1% penicillin-streptomycin (10,000 U mL^{-1} penicillin and 10 mg/mL streptomycin, Solarbio life science, Beijing China).

The cell cytotoxicity of BC-OH and BC-H_2O_2 to HeLa and HepG2 cells were measured by 3-(4,5-dimethylthiazol-2-yl)-2,5-diphenyltetrazolium bromide (MTT) assay. The cytotoxicity was evaluated by Cell Counting Kit-8 (Dojindo, Tokyo, Japan) according to the factory's instruction. Cells were plated in 96-well plates in 0.1 mL volume of DMEM or RPMI-1640 medium with 10 % FBS, at a density of 1×10^4 cells/well and added with desired concentrations of BC-OH and BC-H_2O_2. After incubation for 24 h, absorbance was measured at 490 nm with a Tecan GENios Pro multifunction reader (Tecan Group Ltd., Maennedorf, Switzerland). Each concentration was measured in triplicate and used in three independent experiments. The relative cell viability was calculated by the equation: cell viability (%) = $(OD_{treated}/OD_{control}) \times 100\%$.

In Vitro Cellular Imaging

The A549 cells at 1×10^5 cells/well were seeded onto glass-bottom petri dishes with complete medium (1.0 mL) for 12 h. To explore the effect of H_2O_2 in vitro, the cells were divided into three groupd: The first group of cells served as a reference; The second group of cells were incubated with APAP (500 μM) for 4 h; The third group of mice were incubated with APAP (500 μM) and N-acetyl cysteine (NAC, 500 μM) for 4 h. Subsenquently, three groups of cells were incubated with BC-H_2O_2 (20 μM) for 1 h. After washing the culture dishes three times with PBS, NIR-II fluorescence imaging was conducted with a confocal laser scanning microscope photometrics prime 95B. Filter: 900 nm long-pass; Exposure time: 1000 ms; Laser: 808 nm.

Animal models of Drug Induced Hepatotoxicity

All animal studies were conducted with the approval of the Animal Care and Use Committee in accordance with the guidelines for the care and use of Laboratory Animals. BALB/c female nude mice aged 5-6 weeks were purchased from Shanghai Slac Laboratory Animal Co. Ltd, and kepted under standard conditions. Number of qualitative qualification: No. 20170005045288. Production Permit No.: SCXK (Shanghai) 2017-0005. We randomly divided the mice into three groups: The first group of mice were given an intraperitoneal injection of PBS (200 μL) for 4 h; The second group of mice were intraperitoneally injected with APAP (300 mg kg^{-1}) for 4 h; The third group of mice were administered an

intraperitoneal injection of N-acetyl cysteine (NAC, 300 mg Kg^{-1}), and then given an intraperitoneal injection of APAP (300 mg kg^{-1}) for 4 h. Subsenquently, BC-H_2O_2-loaded nanoparticles in PBS were intravenously (200 μL, 500 μM) injected into the petreated mice. We then conducted the real-time NIR-II fluorescence imaging at different time points after BC-H_2O_2 injection. After the vivo imaging, all three groups of mice were sacrificed to dissect and image the tumor and organs including heart, spleen, kidney and lung. NIR-II fluorescence imaging was conducted with a NIR-II in vivo imaging system MARS. Filter: 1000 nm long-pass; Exposure time: 500 ms; Laser: 808 nm; Laser power: 0.03 W cm^{-2}.

Histology Staining Assays

We fixed the livers of the three groups of mice as metioned above with 10% PFA for 48 h. Subsequently, the samples were dehydrated by ethanol, embedded in paraffin and sectioned. Then, following the satndard protocols of hematoxylin and eosin staining, we prepared the H&E staining samples of livers.

Synthetic method

The 1,3-dimethyl-BODIPY core was synthesized according to the reported method.[1]

Chromene-OH and FC-OH were synthesized by the established procedures from our group.[2]

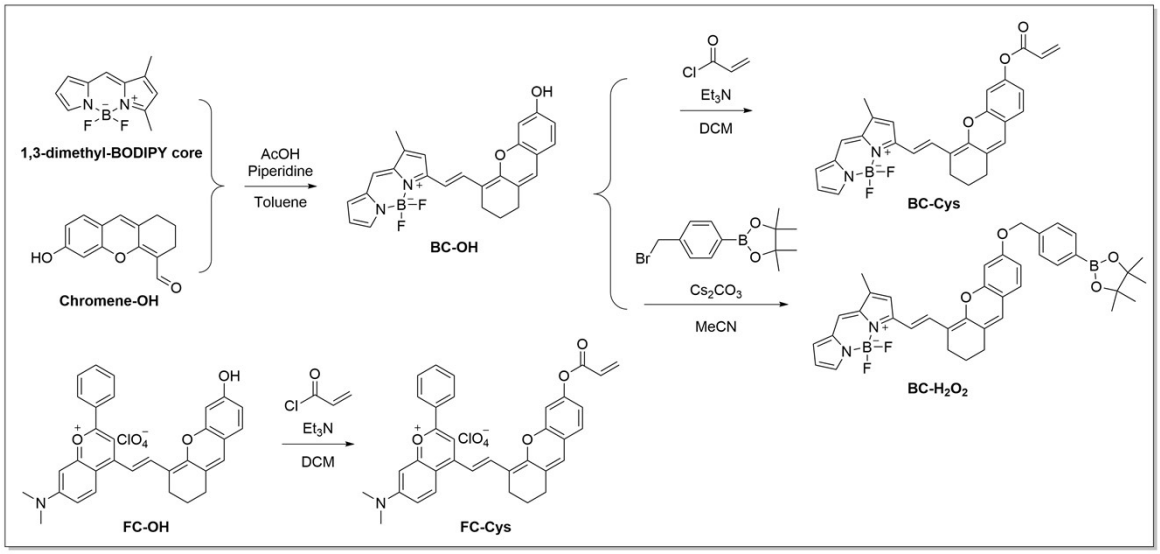

Scheme S1. Synthetic route of BC-OH, BC-Cys, BC-H_2O_2 and the reference FC-Cys.

Synthesis of BC-OH

1,3-dimethyl-BODIPY core was synthesized according to the previous work. Chromene-OH was synthesized according to our previous work mentioned above. 1,3-dimethyl-BODIPY core (23 mg, 0.105 mmol) and Chromene-OH (20 mg, 0.088 mmol) were dissolved in toluene (3.0 mL) along with acetic acid (0.05 mL) and piperidine (0.1 mL). Then the mixture was stirred at 120 ℃ for 4 h under an argon atmosphere. After cooling to room temperature, the solvent was removed under reduced pressure. Then the crude product was purified by silica gel chromatography using Petroleum ether/dichloromethane (v/v, 2 : 3) as the eluent to afford BC-OH as a furvous solid (14 mg): Yield 37%. ^{1}H-NMR (400

Hz, DMSO-d_6, ppm): δ = 1.75 (s, 2H, -CH_2-), 2.32 (s, 3H, -CH_3), 2.45 (s, 2H, -CH_2-), 2.54 (s, 2H, -CH_2-), 6.42 (m, 1H, Ph-H), 6.57-6.60 (dd, J_1 = 8.3 Hz, J_2 = 2.1 Hz, 1H, Ph-H), 6.78-6.82 (m, 3H, Ph-H), 6.90 (d, J = 3.3 Hz, 1H, Ph-H), 7.13 (d, J = 8.3 Hz, 1H, Ph-H), 7.24 (s, 1H, Ph-H), 7.49 (s, 2H, Ph-H), 8.03 (d, J = 15.6 Hz, 1H, alkene-H). ^{13}C-NMR (100 Hz, DMSO-d_6, ppm): δ = 11.11, 20.36, 24.13, 28.67, 102.16, 111.27, 111.71, 112.76, 113.80, 114.99, 118.53, 120.04, 122.81, 125.59, 126.07, 127.52, 132.38, 134.92, 136.24, 138.54, 144.81, 152.68, 153.63, 159.52, 160.02. Mass spectrometry (ESI negative ion mode for $[M - H]^-$): calcd for $C_{25}H_{20}N_2O_2BF_2^-$: 429.1586; found: 429.1592.

Synthesis of BC-Cys

BC-OH (30 mg, 0.070 mmol) and TEA (0.038 mL, 0.280 mmol) were dissolved in dichloromethane (2 mL), and then acryloyl chloride (0.023 mL, 0.280 mmol) was added into the solution. The system was stirred at room temperature for 12 h under argon protection. After reaction was over, the organic layer was then washed with H_2O, dried over Na_2SO_4, filtered and concentrated under vacuum, and then the crude product was purified by silica gel chromatography using Petroleum ether/dichloromethane (v/v, 3 : 1) as the eluent to afford BC-Cys as a furvous solid (25 mg): Yield 74%. ^{1}H-NMR (400 Hz, DMSO-d_6, ppm): δ = 1.76-1.79 (m, 2H, -CH_2-), 2.32 (s, 3H, -CH_3), 2.45-2.50 (m, 2H, -CH_2-), 2.57-2.59 (m, 2H, -CH_2-), 6.20-6.23 (dd, J_1 = 10.3 Hz, J_2 = 1.2 Hz, 1H, Ph-H), 6.41-6.48 (m, 2H, Ph-H), 6.56-6.61 (m, 1H, Ph-H), 6.83-6.87 (m, 2H, Ph-H), 6.94-6.97 (m, 2H, Ph-H), 7.25 (s, 1H, Ph-H), 7.30 (d, 1H, J = 2.2 Hz, Ph-H), 7.34 (d, 1H, J = 8.3 Hz, Ph-H), 7.55 (s, 1H, Ph-H), 7.59 (s, 1H, Ph-H). 8.04 (d, J = 15.8 Hz, 1H, alkene-H). ^{13}C-NMR (100 Hz, DMSO-d_6, ppm): δ = 11.61, 20.67, 24.36, 29.29, 109.81, 112.99, 114.60, 115.95, 117.67, 118.82, 120.24, 121.90, 124.14, 124.42, 127.55, 127.84, 130.50, 133.06, 134.66. 136.09, 136.49, 138.81, 145.50, 151.24, 151.73, 153.05, 160.12, 164.38. Mass spectrometry (ESI positive ion mode for $[M + H]^+$): calcd for $C_{28}H_{24}N_2O_3BF_2^+$: 485.1848; found: 485.1847.

Synthesis of BC-H_2O_2

BC-OH (30 mg, 0.070 mmol), 4-(Bromomethyl)benzeneboronic acid pinacol ester (31 mg, 0.105 mmol) and Cs_2CO_3 (72 mg, 0.210 mmol) were dissolved in acetonitrile (2 mL) and the system was stirred at room temperature for 12 h under argon protection. After reaction was over, the mixture was filtered and concentrated under vacuum, and then the crude product was purified by silica gel chromatography using Petroleum ether/dichloromethane (v/v, 3 : 1) as the eluent to afford BC-H_2O_2 as a furvous solid (16 mg): Yield 36%.^{1}H-NMR (400 Hz, DMSO-d_6, ppm): δ = 1.30 (s, 12H, -$C(CH_3)_4$), 1.75-1.78 (m, 2H, -CH_2-), 2.34 (s, 3H, -CH_3), 2.46-2.47 (m, 2H, -CH_2-), 2.55-2.57 (m, 2H, -CH_2-), 5.22 (s, 2H, -OCH_2-), 6.42-6.44 (m, 1H, Ph-H), 6.80-6.86 (m, 3H, Ph-H), 6.93 (d, J = 8.3 Hz, 1H, Ph-H), 7.16 (d, J = 2.3 Hz, 1H, Ph-H), 7.24-7.26 (m, 2H, Ph-H), 7.49-7.52 (m, 3H, Ph-H), 7.55 (s, 1H, Ph-H), 7.73 (d, J = 8.0 Hz, 2H, Ph-H), 8.05 (d, J = 15.7 Hz, 1H, alkene-H). ^{13}C-NMR (100 Hz, DMSO-d_6, ppm): δ = 11.62, 20.79, 25.14, 25.41, 29.20, 69.94, 73.99, 84.18, 102.25, 111.63, 112.17, 113.77, 115.71, 115.81, 118.79, 121.11, 123.81, 125.37, 127.41, 127.82, 127.91, 128.72, 132.96, 134.85, 135.08, 135.87, 136.45, 138.94, 140.37, 145.44, 152.75, 153.95, 160.29. Mass spectrometry (ESI positive ion mode for $[M + H]^+$): calcd for $C_{38}H_{39}N_2O_4B_2F_2^+$: 647.3064; found: 647.3054.

Synthesis of FC-Cys

FC-OH was synthesized according to our previous work mentioned above. FC-OH (40 mg, 0.070 mmol) and TEA (0.038 mL, 0.280 mmol) were dissolved in dichloromethane (2 mL), and then acryloyl chloride (0.023 mL, 0.280 mmol) was added into the solution. The system was stirred at room temperature for 12 h under argon protection. After reaction was over, the organic layer was then washed with H_2O, dried over Na_2SO_4, filtered and concentrated under vacuum, and then the crude product was purified by silica gel chromatography using dichloromethane/methanol (v/v, 99 : 1) as the eluent to afford FC-Cys as a furvous solid (30 mg): Yield 68%. ^{1}H NMR (400 MHz, DMSO-d_6, ppm): δ = 1.83-1.86 (m, 2H, -CH_2-), 2.68-2.77 (m, 4H, -CH_2-), 3.27 (s, 6H, -$N(CH_3)_2$), 6.25-6.27 (dd, J_1 = 10.3 Hz, J_2 = 1.2 Hz, 1H, alkene-H), 6.46-6.52 (m, 1H, alkene-H), 6.60-6.65 (m, 1H, alkene-H), 7.09-7.10 (d, J = 2.5 Hz, 1H, Ph-H), 7.12-7.14 (dd, J_1 = 8.4 Hz, J_2 = 2.2 Hz, 1H, Ph-H), 7.23-7.26 (m, 2H, Ph-H), 7.28-7.32 (d, J = 14.9 Hz, 1H, alkene-H), 7.48-7.49 (d, J = 2.1 Hz, 1H, Ph-H), 7.52-7.54 (d, J = 8.4 Hz, 1H, Ph-H), 7.65-7.73 (m, 3H, Ph-H), 8.22 (s, 1H, Ph-H), 8.37-8.40 (m, 2H, Ph-H), 8.45-8.47 (d, J = 9.8 Hz, 1H, Ph-H), 8.69-8.72 (d, J = 14.8 Hz, 1H, alkene-H). ^{13}C NMR (100 MHz, DMSO-d_6, ppm): δ = 19.89, 24.10, 28.66, 96.69, 102.34, 109.85, 112.93, 114.73, 115.10, 115.47, 118.58, 119.68, 127.15, 127.24, 127.81, 128.78, 129.24, 129.88, 130.26, 132.72, 134.61, 140.78, 151.45, 152.24, 152.50, 155.63, 156.56, 157.01, 160.48, 163.97. Mass spectrometry (ESI positive ion mode for $[M - ClO_4]^+$): calcd for $C_{35}H_{30}NO_4^+$: 528.2175; found: 528.2171.

Table S1. Representative activatable NIR-II fluorescent probes

Probes	Analyte	Photochemical designed mechanism	λ_{abs}	λ_{fl}	Imaging applications	Ref.
NIR-II@Si	H_2S	Target-induced change in the chemical structures of fluorescent probes	780	900	The sensitive identification of colon cancer tumor in vivo	3
Hydro-1080	•OH	Target-induced change in the chemical structures of fluorescent probes	1021	1044	Monitor •OH induced by LPS and APAP overdose	4
PN1100	$ONOO^-$	Förster resonance energy transfer (FRET)	1089	920/ 1130	APAP-induced hepatotoxicity monitoring	5
PN910	ROS/RNS and base	intramolecular charge transfer (ICT)	870	910	Monitoring cystitis and colitis	6
Benz-NorCys7	pH	Target-induced change in the chemical structures of fluorescent probes	1130	1275	Ratiometric pH imaging in vivo	7
LC-1250	H_2O_2	Target-induced change in the chemical structures of fluorescent probes	1150	1250	Ratiometric monitoring of the intestinal inflammation and the excised stomach	8
NIR-II-F3LAP	aminopeptidase (LAP)	Target-induced change in the chemical structures of fluorescent probes	760	1040	LAP change in drug-induced liver injury mice	9

1. Photophysical properties of BC-OH

Table S2. Photophysical properties of BC-OH

Dye	MW (g mol^{-1})	λ_{abs} (nm)	ε (M^{-1} cm^{-1})	λ_{fl} (nm)	Φ_{fl} (%)
BC-OH	430	790	54300	905	0.13[a]

Measured in pH 7.4 PBS/DMSO (1:1, v:v). [a]Fluorescence quantum efficiency (Φ_{fl}) was determined using IR26 as a reference (Φ_{fl} = 0.05%, dichloroethane).

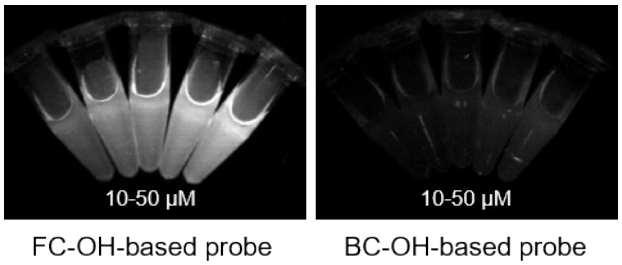

Fig. S1. NIR-II fluorescent images of FC-OH/BC-OH-based probes at different concentrations (10-50 μM) on a NIR-II imaging system (Laser: 808 nm; Exposure time: 100 ms; Filter: 1000 nm long-pass).

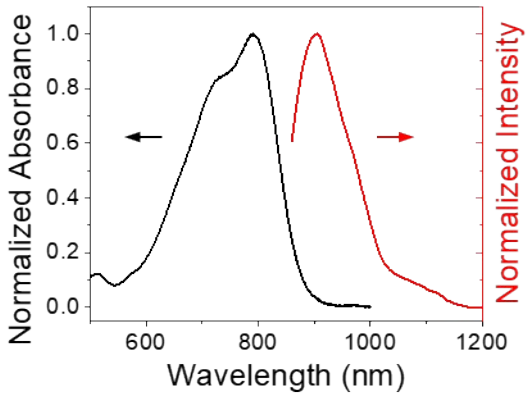

Fig. S2. Normalized absorption and emission spectra of BC-OH in PBS/DMSO solution (pH 7.4, 1:1, v/v).

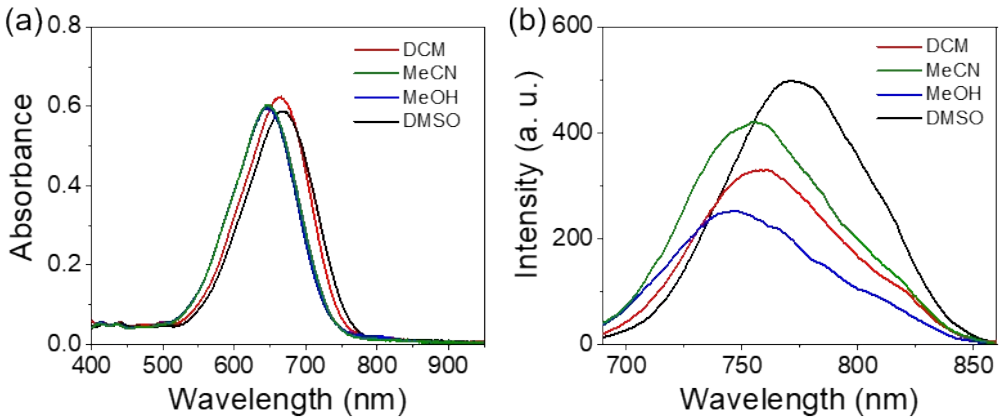

Fig. S3. The absorption spectra (a) and fluoresence spectra (b) of BC-OH (10 μM) in different solvents, λ_{ex} = 650 nm.

2. Determination of p*K*a value of BC-OH

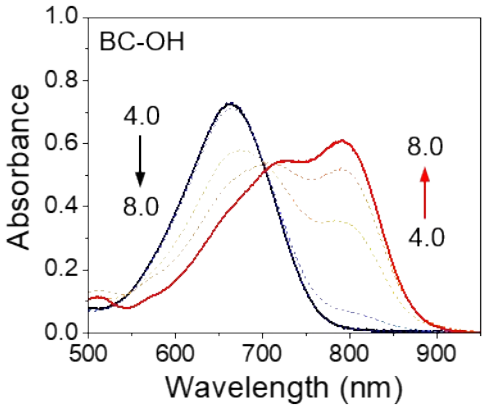

Fig. S4. pH-dependent absorption spectra of BC-OH (10 μM) in Britton-Robinson buffer/DMSO solution (1:1, v/v).

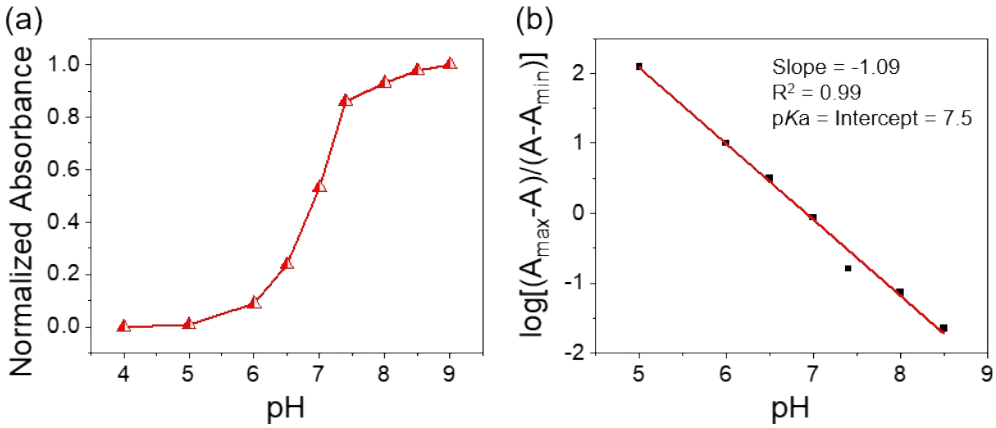

Fig. S5. (a) pH-dependent normalized absorption intensity at 790 nm of BC-OH (10 μM) in PBS/DMSO solution (1:1, v/v). (b) The relationship between Log[(A_{max}-A)/(A-A_{min})] of BC-OH and pH value. A represents the observed absorbance at 790 nm, A_{max} and A_{min} represent the maximum and minimal absorbance, respectively.

3. Stability of BC-OH

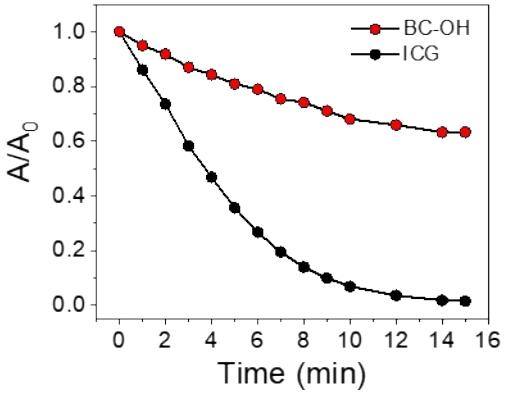

Fig. S6. Photostability of BC-OH and ICG (10 μM) under 808 nm laser with a power density of 1 W cm^{-2} in PBS/DMSO solution (pH 7.4, 1:1, v/v).

For the photostability test, time-dependent absorption measurements were conducted under light irradiation (1 W cm^{-2}). After stable light irradiation for 15 min, the absorbance of the commercially FDA-proved cyanine dye ICG quickly dropped to 1%, while the decrease of BC-OH was merely approximately 70%.

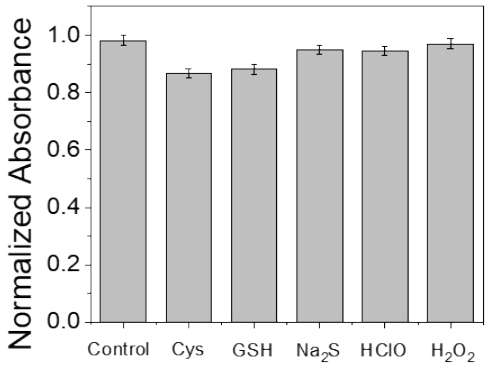

Fig. S7. The normalized absorbance of BC-OH (10 μM) at 790 nm in PBS/DMSO (pH 7.4, 1:1, v/v) after incubation with various species (100 μM Cys; GSH; Na_2S; HClO; H_2O_2) at 37 ºC for 1 h.

After incubation with various species at 37 °C for 1 h, we evaluated the chemical stability of BC-OH by absorption spectral analysis.

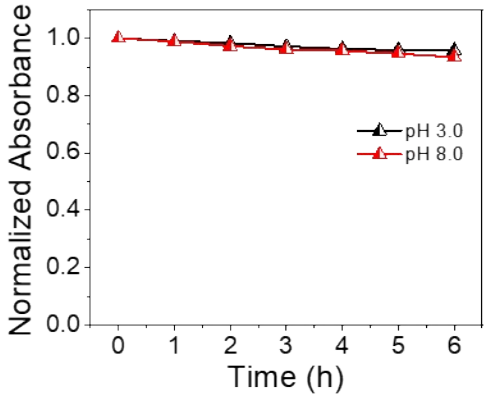

Fig. S8. Time-dependent normalized absorption intensity at 660 or 790 nm of BC-OH (10 μM) in PBS/DMSO solution (1:1, v/v). pH = 3.0 or 8.0.

4. Sensing mechanism

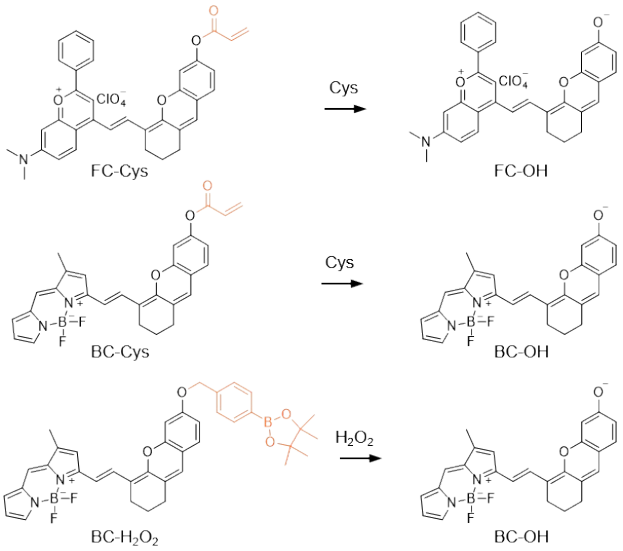

Fig. S9. Sensing mechanism of FC-Cys, BC-Cys and BC-H_2O_2.

5. Theoretical calculations

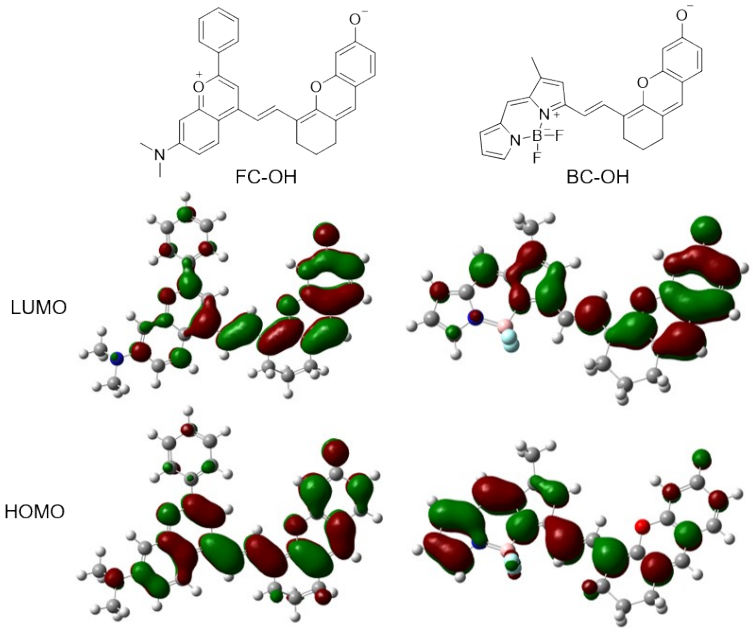

Fig. S10. Molecular orbital plots (HOMO and LUMO) of FC-OH and BC-OH.

Results show that the π-conjugated "crossbreeding" dyes (FC-OH and BC-OH) possess effective conjugative chain within little bond-length alternation and bear strong electronic delocalization in their molecular structure. Specifically, electron-hole analysis reveals that BC-OH demonstrates more significant intramolecular charge transfer (ICT) process compared to FC-OH upon photoexcitation. Thus, enhancing the electron-donating ability of hydroxyl in BC-OH-based probes endows a larger absorption spectral separation with analytes than that of FC-OH-based probes.

6. The Kinetics curve of BC-Cys reaction at 905 nm

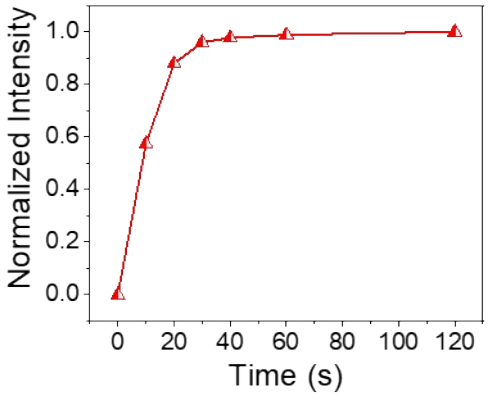

Fig. S11. Time dependence of fluorescence intensity at 905 nm for BC-Cys (10 μM) in pH 7.4 PBS/DMSO (1:1, v:v) in the presence of Cys. λ_{ex} = 808 nm

7. The linear relationship between fluorescence intensity and concentration of Cys

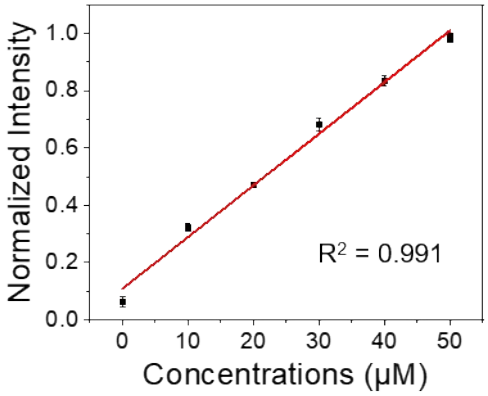

Fig. S12. The linear relationship between fluorescence intensity of BC-Cys at 905 nm and Cys concentration.

8. Selectivity of the BC-Cys

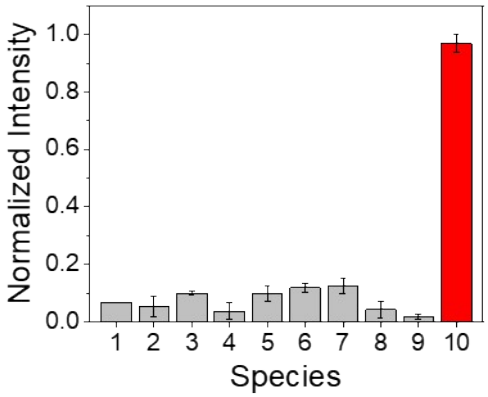

Fig. S13. Fluorescence response of BC-Cys (10 μM) toward various analytes (from 1 to 10): blank, GSH (100 μM), Glycine (100 μM), $ONOO^-$ (50 μM), NaClO (100 μM), H_2O_2 (100 μM), $HO^\bullet$ (100 μM), $O_2^{\bullet-}$ (100 μM), Na_2S (100 μM), Cys (100 μM).

9. The linear relationship between fluorescence intensity and concentration of H_2O_2

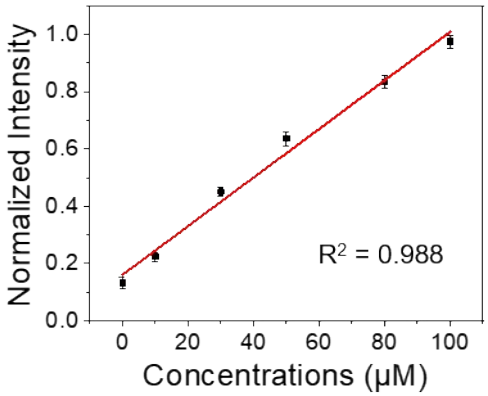

Fig. S14 The linear relationship between fluorescence intensity of BC-H_2O_2 at 905 nm and H_2O_2 concentration.

10. The Kinetics curve of BC-H_2O_2 reaction at 905 nm

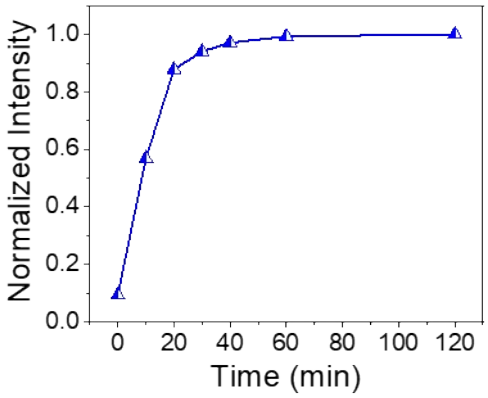

Fig. S15. Time dependence of fluorescence intensity at 905 nm for BC-H_2O_2 (10 μM) in pH 7.4 PBS/DMSO (1:1, v:v) in the presence of H_2O_2. λ_{ex} = 808 nm

11. Selectivity of the BC-H_2O_2

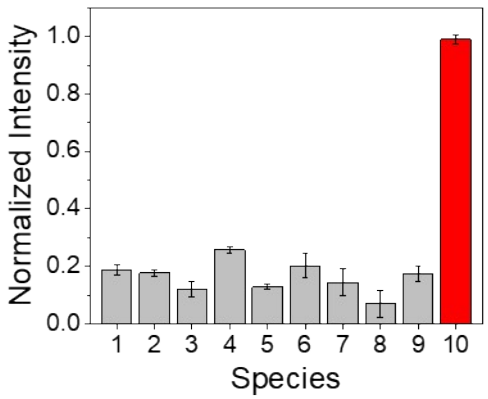

Fig. S16. Fluorescence response of BC-H_2O_2 (10 μM) toward a series of species (from 1 to 10, 100 μM): blank, GSH, Glycine, $ONOO^-$, NaClO, Cys, $HO^{\bullet}$, $O_2^{\bullet-}$, Na_2S, H_2O_2.

12. HPLC chromatogram of BC-H_2O_2 and BC-OH

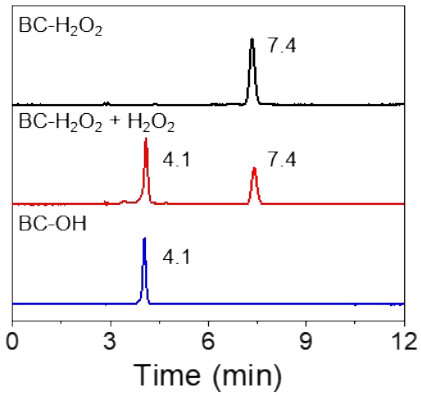

Fig. S17. HPLC chromatogram of BC-H_2O_2 before and after reaction with H_2O_2, and BC-OH. Eluent solvent: methanol; Detection wavelength: 650 nm; Flow rate: 1 mL min^{-1}.

The retention time of BC-H_2O_2 and BC-OH was about 7.4 and 4.1 min, respectively. Obviously, after the mixture of BC-H_2O_2 with H_2O_2 was kept for 20 min, a retention peak at about 4.1 min appeared, corresponding to that of BC-OH.

13. Preparation of H_2O_2-loaded nanoparticles

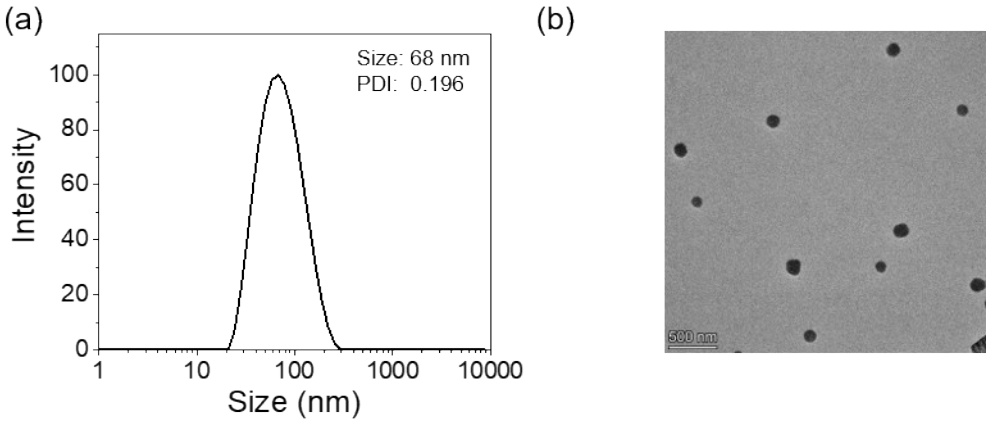

Fig. S18 (a) Size distribution of BC-H_2O_2-loaded nanoparticles in aqueous solution at pH 7.4. (b) TEM images of BC-H_2O_2-loaded nanoparticles.

14. Cytotoxicity of BC-OH and BC-H_2O_2

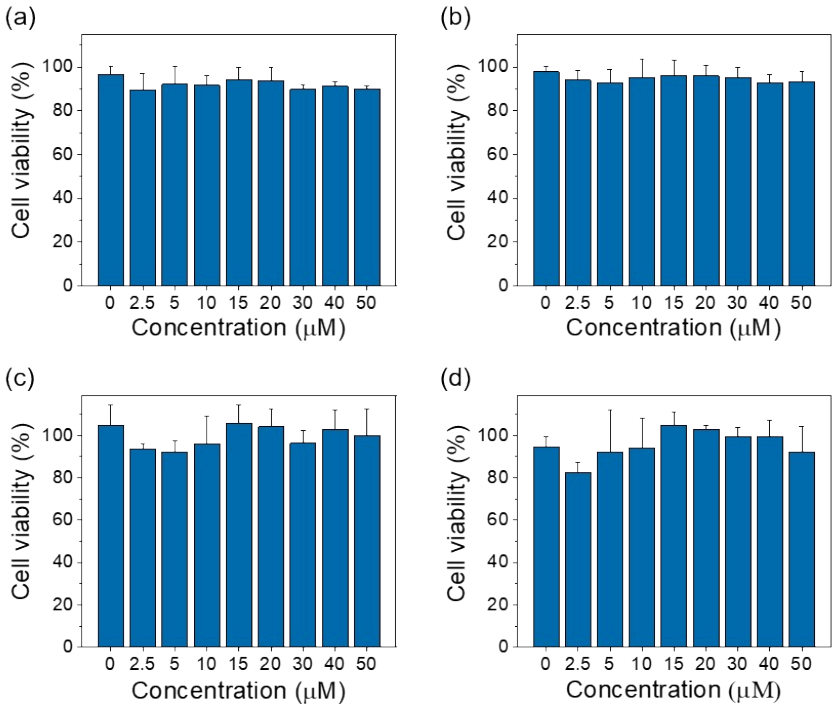

Fig. S19. Relative viability of HeLa (a, b) and HepG2 (c, d) cells in vitro after incubation for 24 h with BC-OH (a, c) and BC-H_2O_2 (b, d) at various concentrations. Note: both BC-OH and BC-H_2O_2 have minimal toxicity and enjoy superior biocompatibility toward cultured cell lines.

15. Imaging H_2O_2 in living cells

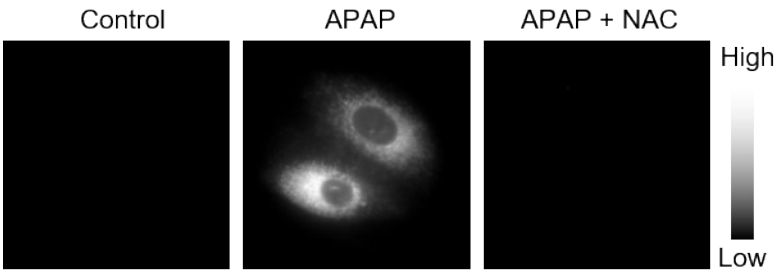

Fig. S20. NIR-II fluorescence images of endogenous H_2O_2 in A549 cells. Control group: the cells were treated with BC-H_2O_2 (20 μM). APAP group: the cells were treated with APAP (500 μM) and then BC-H_2O_2 (20 μM). APAP + NAC group: the cells were treated with APAP (500 μM), NAC (500 μM) and then BC-H_2O_2 (20 μM). Filter: 900 nm long-pass; Exposure time: 1000 ms; Laser: 808 nm.

16. Imaging APAP-induced hepatotoxicity in vivo

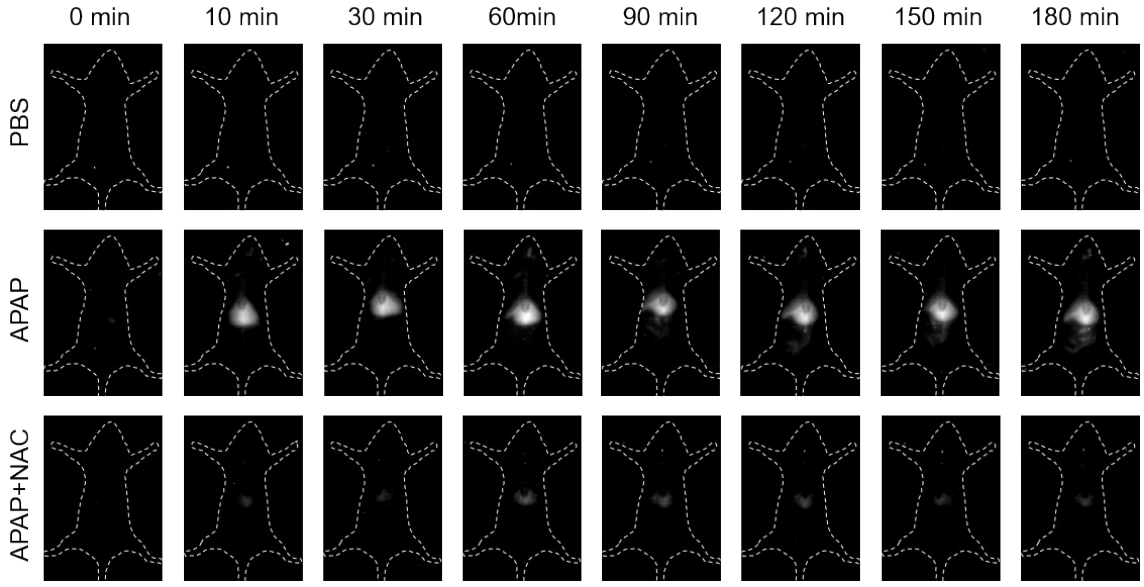

Fig. S21. Time-dependent NIR-II fluorescence imaging in different groups of mice: PBS group, APAP group, and APAP + NAC group.

BALB/c nude mice were given an injection of PBS (200 μL) for 4 h as the control group. To construct the drug-induced liver injury model, mice were administered with an injection of APAP (300 mg kg^{-1}) for 4 h. Moreover, the third group of mice were given an injection of NAC (300 mg kg^{-1}) and APAP (300 mg kg^{-1}). As reported, those doses could efficiently induce and recover inflammation, respectively.[10] Subsequently, we took three groups of mice and performed intravenous injection of BC-H_2O_2-loaded nanoparticles (500 μM) and then performed NIR-II fluorescence imaging in vivo.

References

1. B. Kim, M. Fukuda, J. Y. Lee, D. Su, S. Sanu, A. Silvin, A. T. T. Khoo, T. Kwon, X. Liu, W. Chi, X. Liu, S. Choi, D. S. Y. Wan, S. J. Park, J. S. Kim, F. Ginhoux, H. S. Je and Y. T. Chang, *Angew. Chem. Int. Ed.*, 2019, **58**, 7972-7976.
2. L. Zhang, Y. Zhang, W. Chi, C. Yan, Z. Zhao, X. Liu, W.-H. Zhu and Z. Guo, *ACS Mater. Lett.*, 2022, **4**, 1493-1502.
3. G. Xu, Q. Yan, X. Lv, Y. Zhu, K. Xin, B. Shi, R. Wang, J. Chen, W. Gao, P. Shi, C. Fan, C. Zhao and H. Tian, *Angew. Chem. Int. Ed.*, 2018, **57**, 3626-3630.
4. W. Feng, Y. Zhang, Z. Li, S. Zhai, W. Lv and Z. Liu, *Anal. Chem.*, 2019, **91**, 15757-15762.
5. Z. Lei, C. Sun, P. Pei, S. Wang, D. Li, X. Zhang and F. Zhang, *Angew. Chem. Int. Ed.*, 2019, **58**, 8166-8171.
6. F. Zhang, X. Zhang, Y. Chen, H. He, S. Wang and Z. Lei, *Angew. Chem. Int. Ed.*, 2021, **60**, 26337-26341.
7. S. M. Usama, D. R. Caldwell, P. Shrestha, M. P. Luciano, N. L. Patel, J. D. Kalen, J. Ivanic and M. J. Schnermann, *Biosens. Bioelectron.*, 2022, **217**, 114610.
8. T. Li, K. Cao, X. Yang, Y. Liu, X. Wang, F. Wu, G. Chen and Q. Wang, Biomaterials, 2023, **293**, 121956.
9. X. Zhang, S. Shen, D. Liu, X. Li, W. Shi and H. Ma, *Chem. Sci.*, 2023, **14**, 2928-2934.
10. A. J. Shuhendler, K. Pu, L. Cui, J. P. Uetrecht and J. Rao, *Nat. Biotechnol.*, 2014, **32**, 373–380.

Characterization of BC-OH, BC-Cys, BC-H_2O_2 and FC-Cys

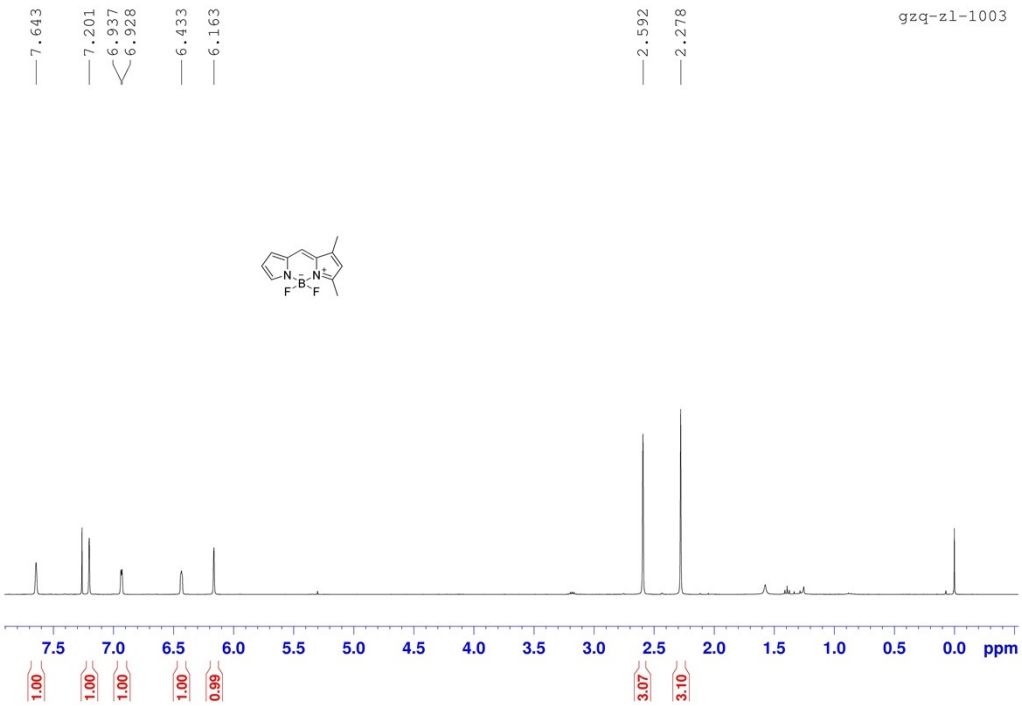

Fig. S22. ^{1}H NMR spectrum of 1,3-dimethyl-BODIPY in $CDCl_3$

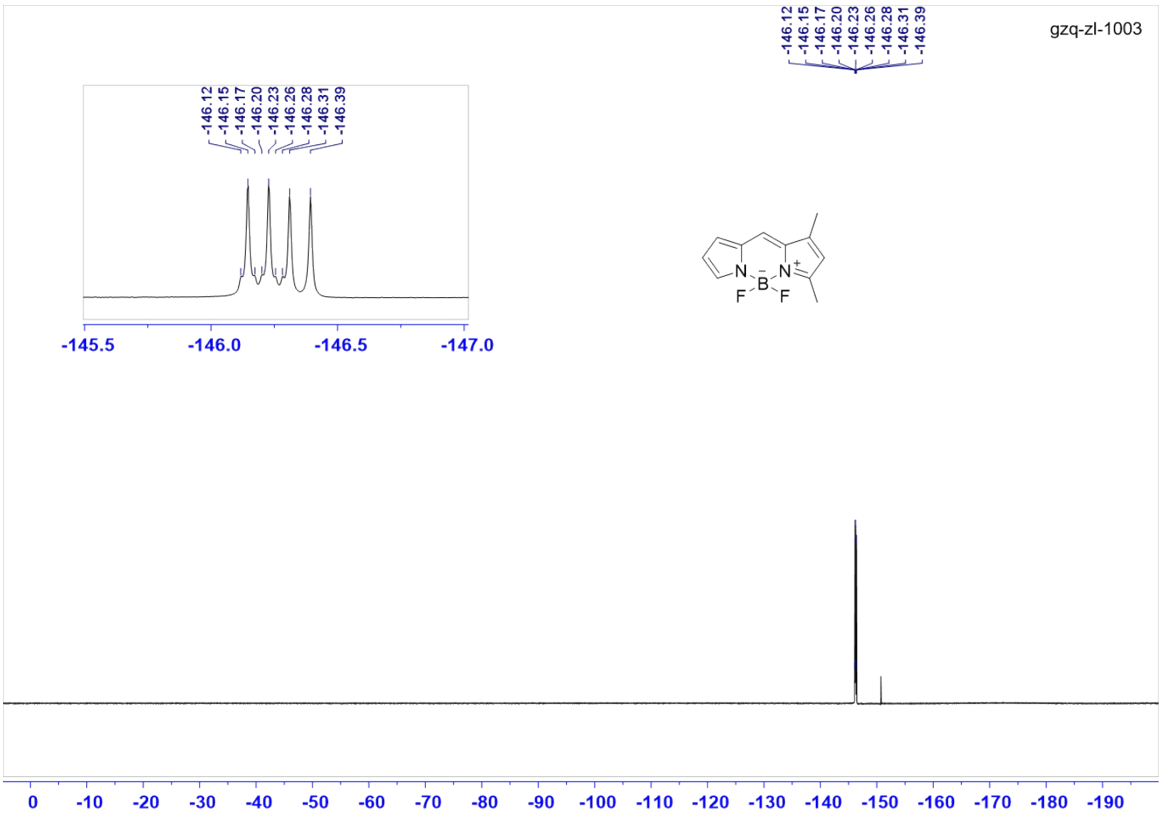

Fig. S23. ^{19}F NMR spectrum of 1,3-dimethyl-BODIPY in $CDCl_3$

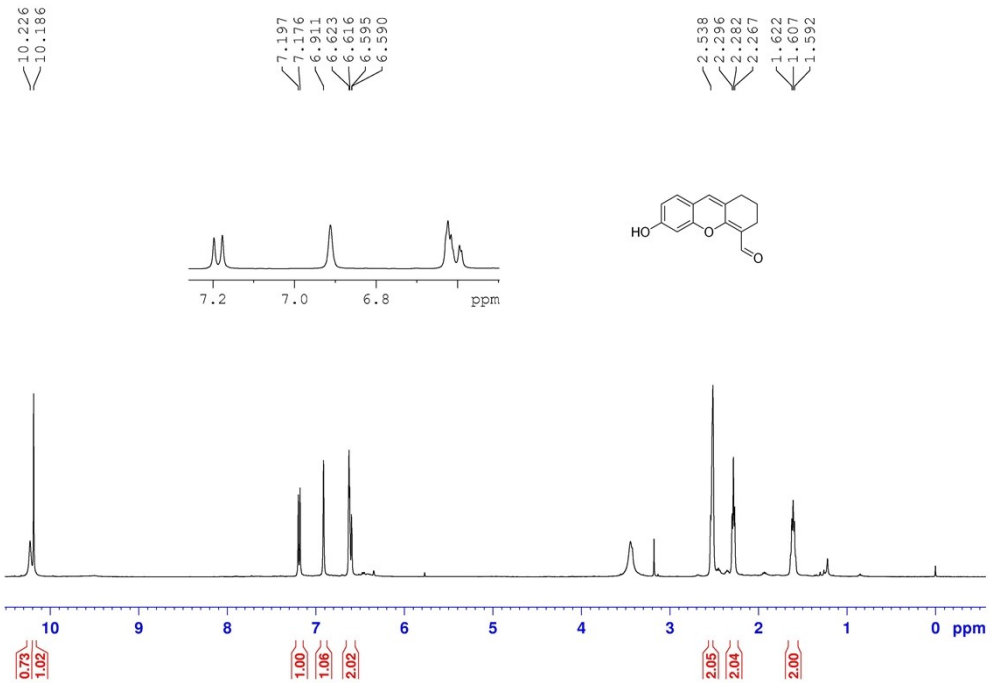

Fig. S24. ^{1}H NMR spectrum of Chromene-OH in DMSO-d_6

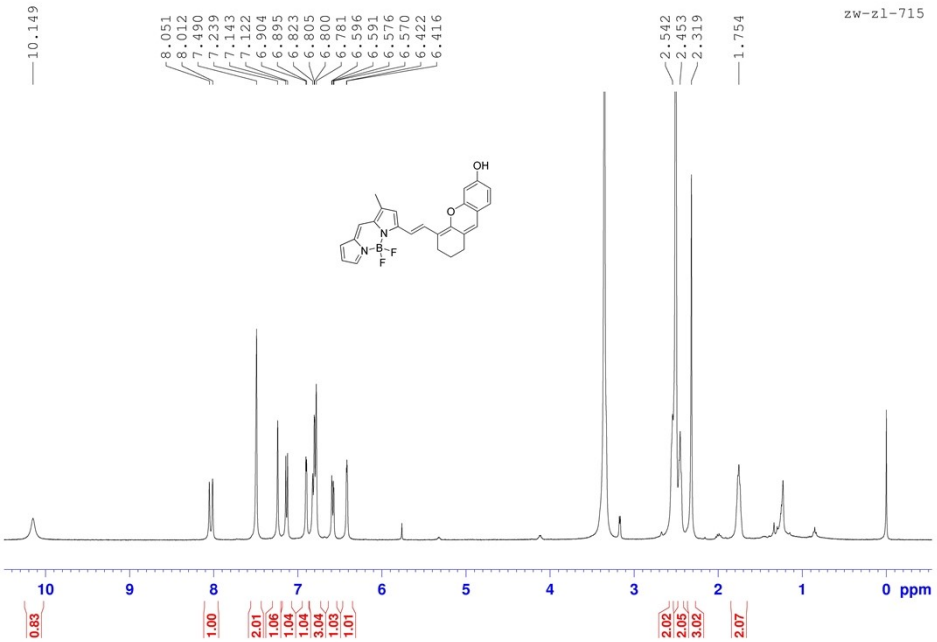

Fig. S25. ^{1}H NMR spectrum of BC-OH in DMSO-d_6

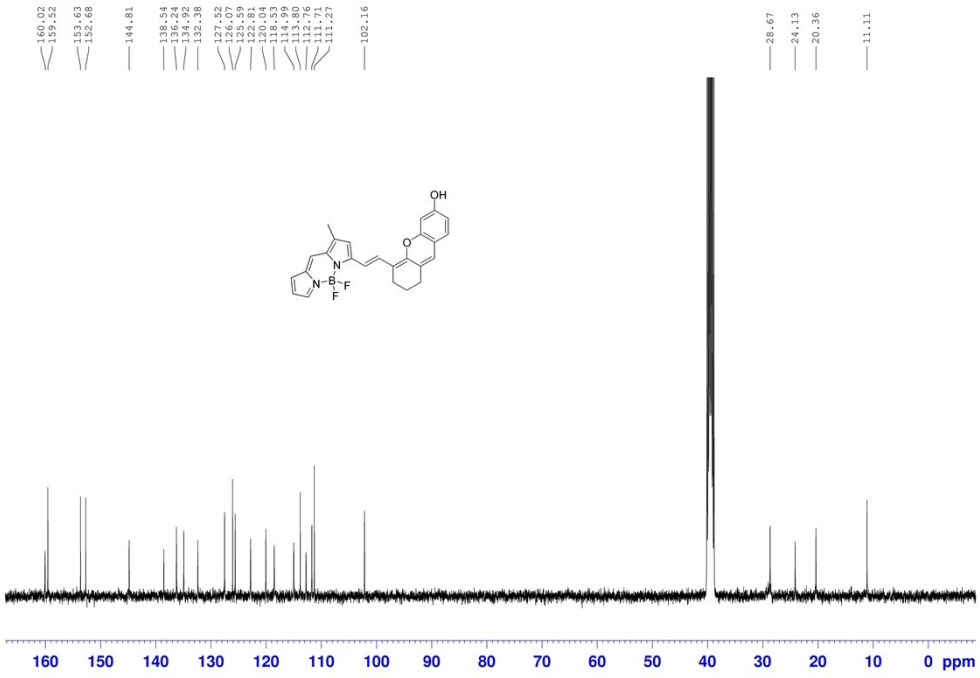

Fig. S26. ^{13}C NMR spectrum of BC-OH in DMSO-d_6

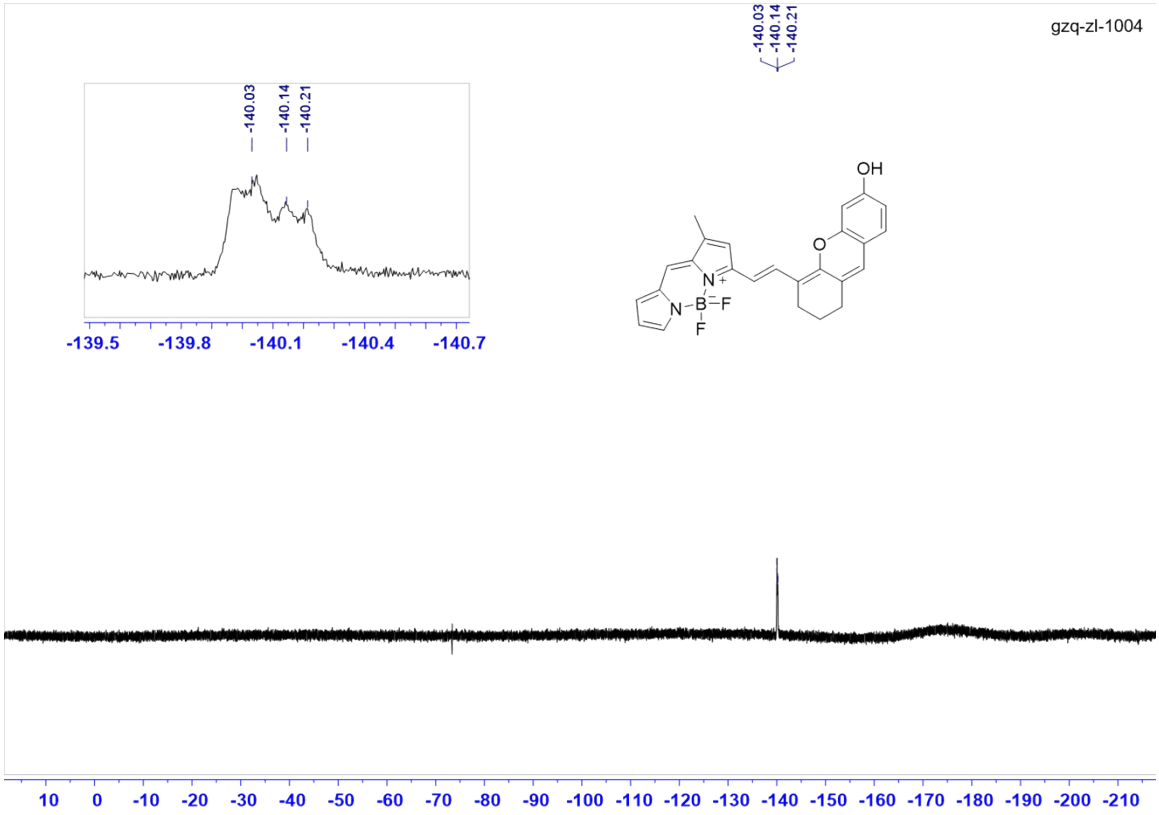

Fig. S27. ^{19}F NMR spectrum of BC-OH in DMSO-d_6

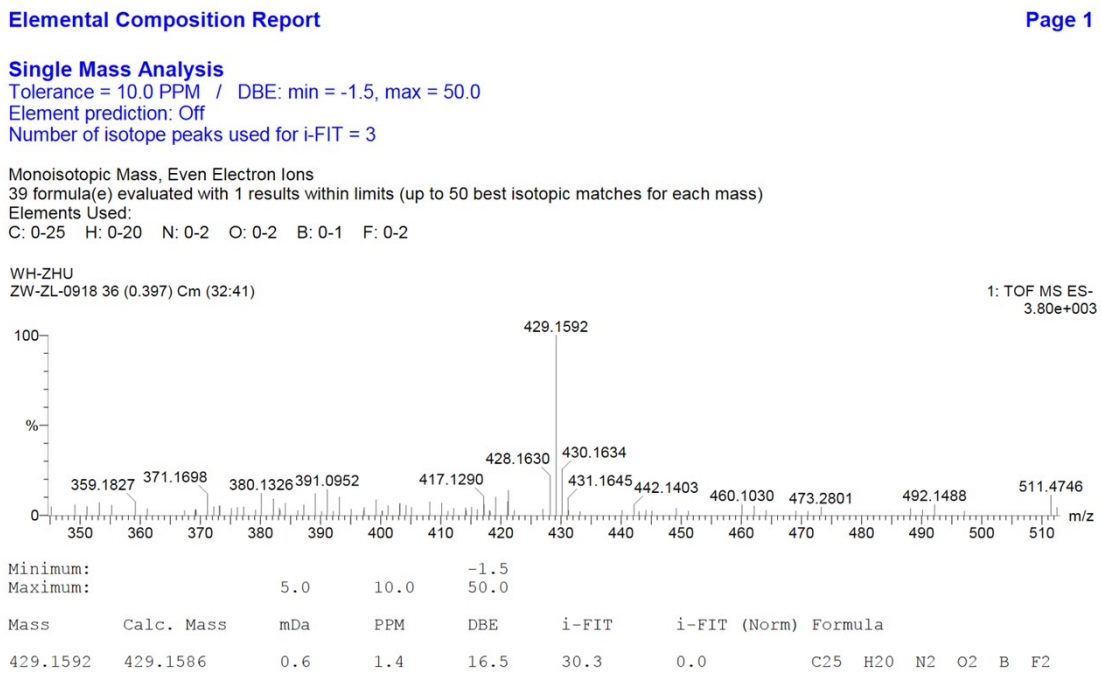

Fig. S28. HRMS spectrum of BC-OH.

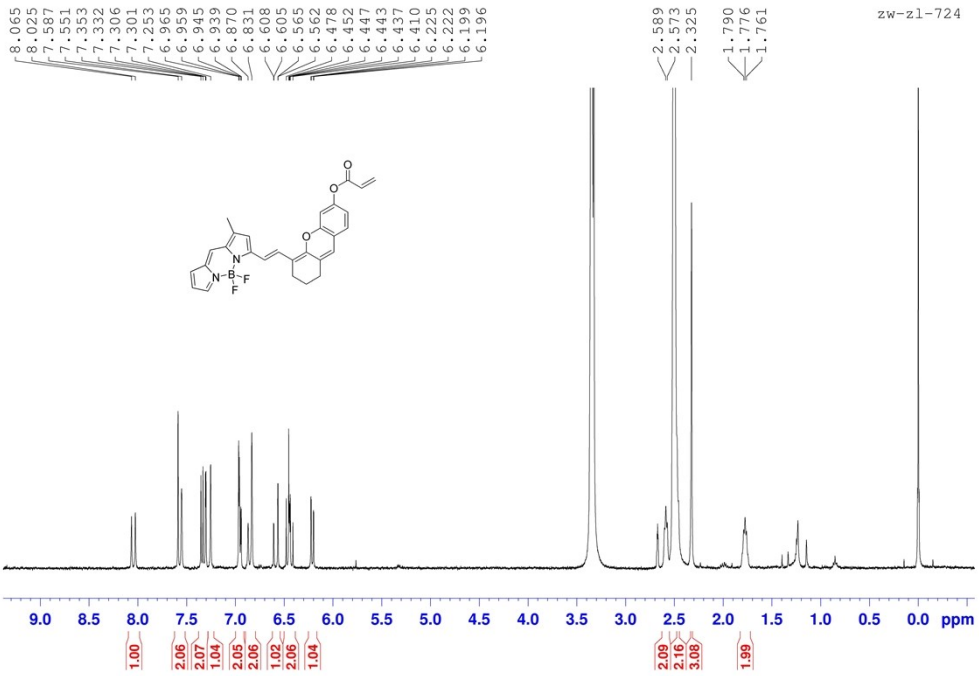

Fig. S29. [1]H NMR spectrum of BC-Cys in DMSO-d_6

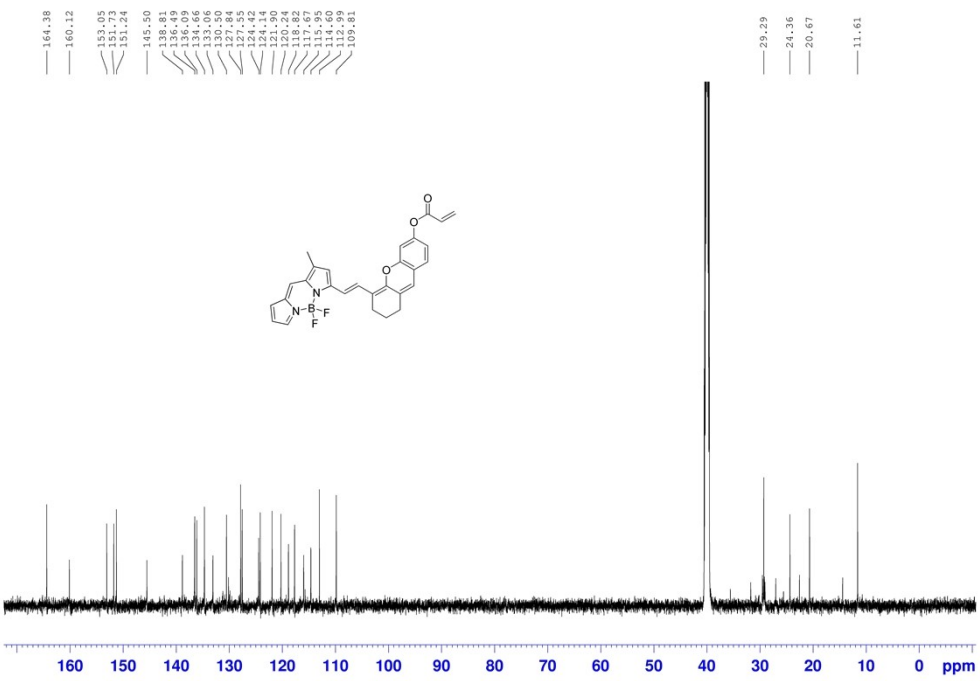

Fig. S30. [13]C NMR spectrum of BC-Cys in DMSO-d_6

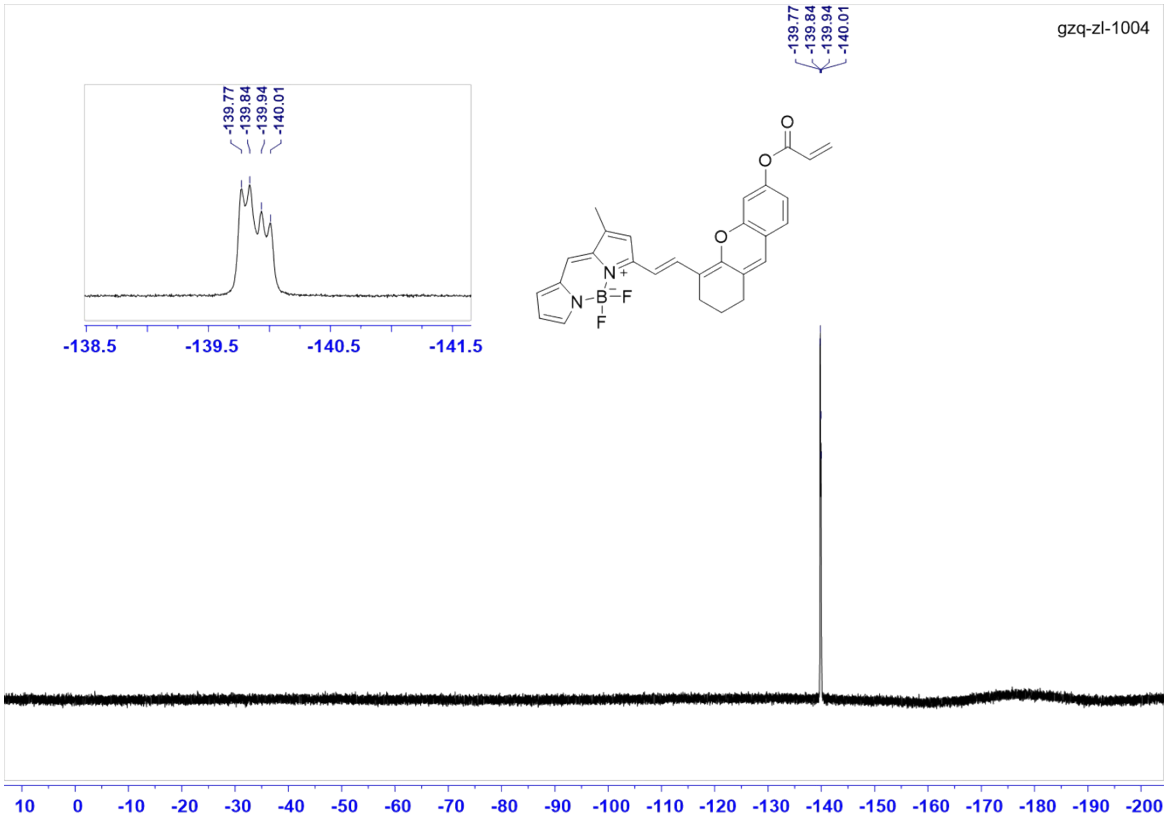

Fig. S31. ^{19}F NMR spectrum of BC-Cys in DMSO-d_6

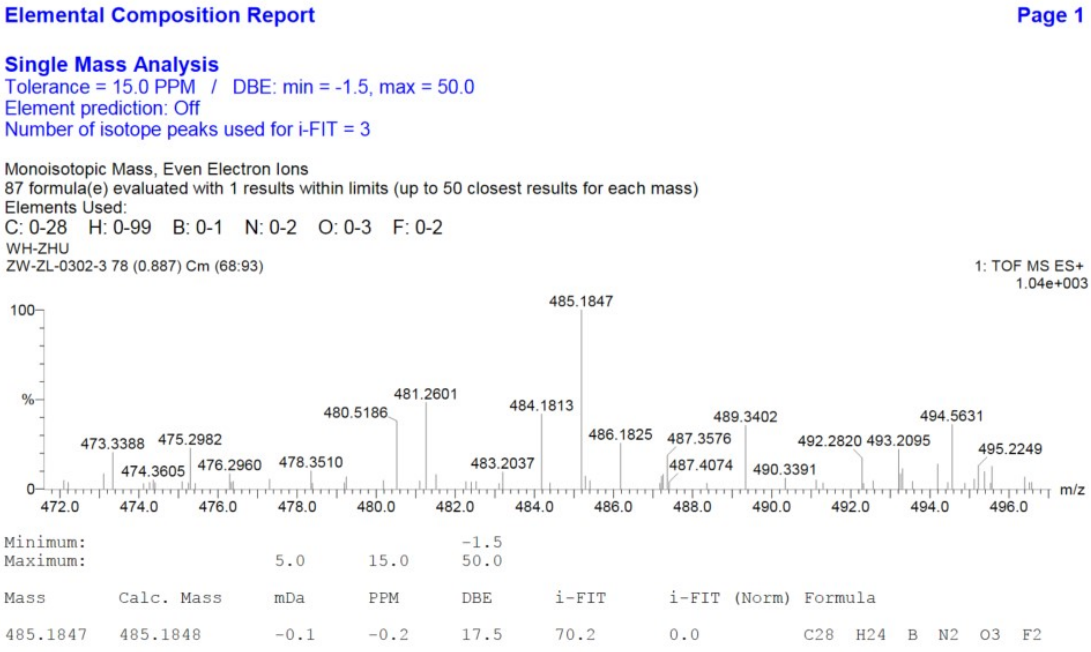

Fig. S32. HRMS spectrum of BC-Cys.

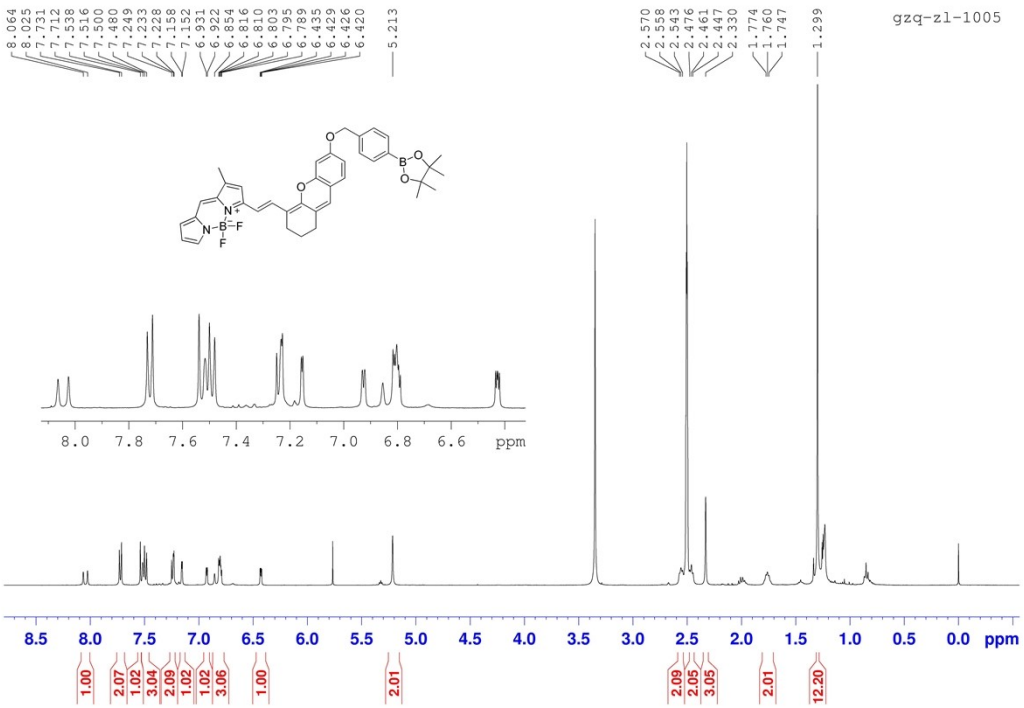

Fig. S33. ^{1}H NMR spectrum of BC-H_2O_2 in DMSO-d_6

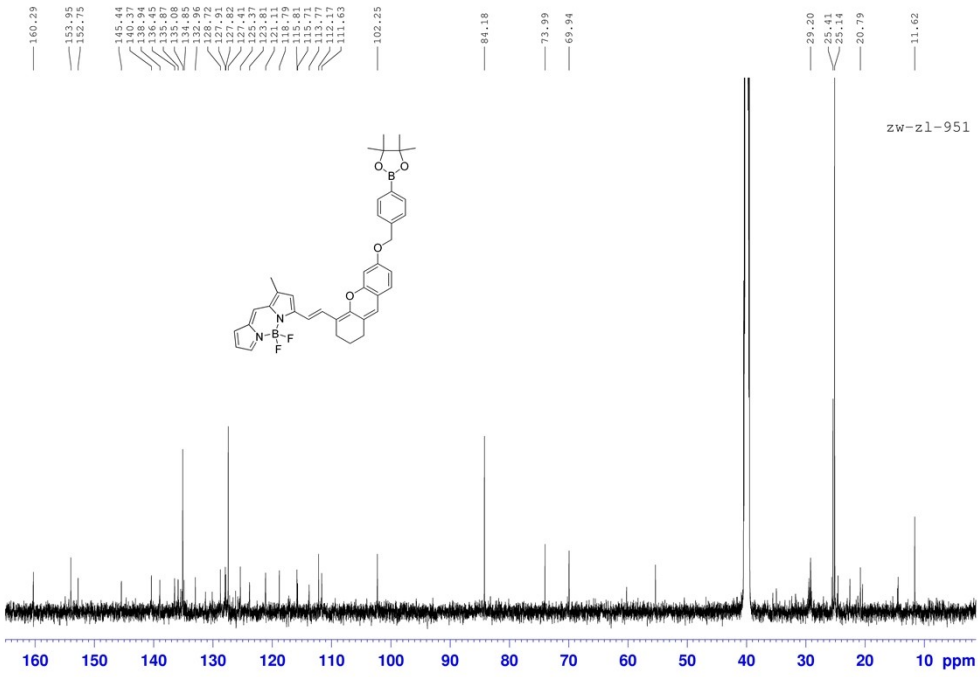

Fig. S34. ^{13}C NMR spectrum of BC-H_2O_2 in DMSO-d_6

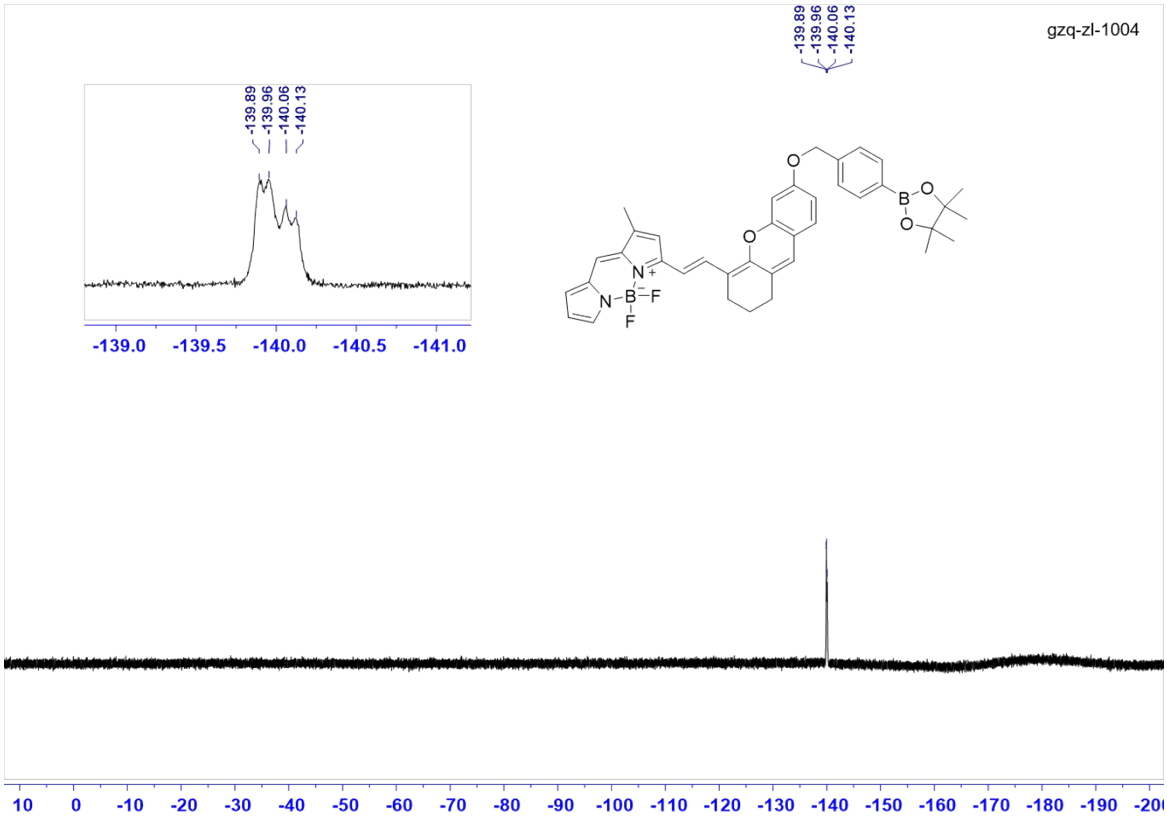

Fig. S35. ^{19}F NMR spectrum of BC-H_2O_2 in DMSO-d_6

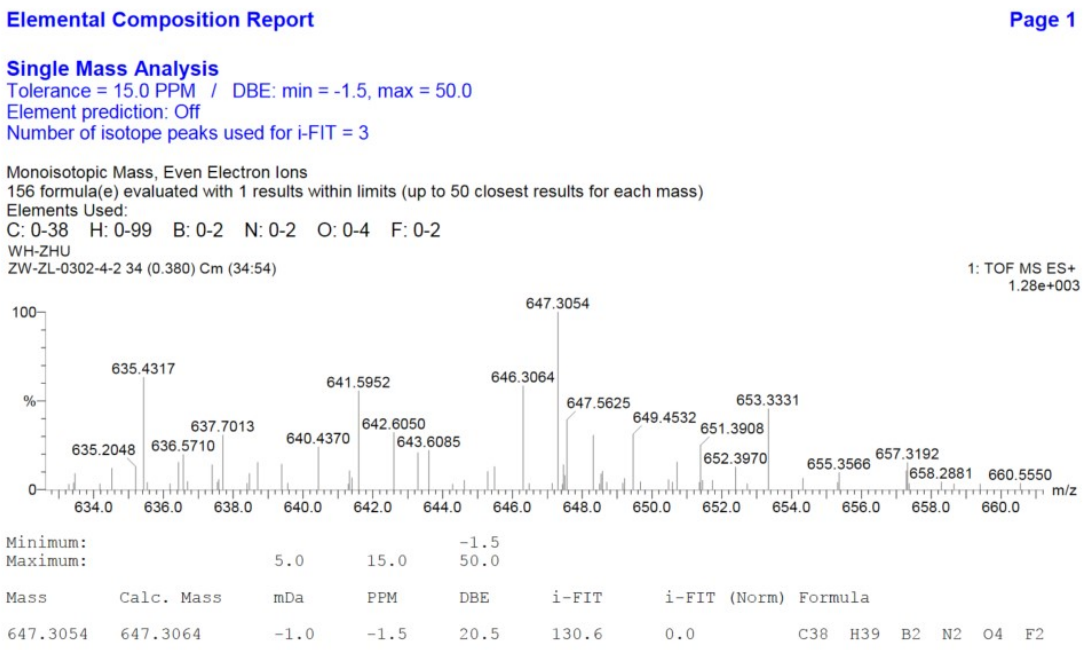

Fig. S36. HRMS spectrum of BC-H_2O_2.

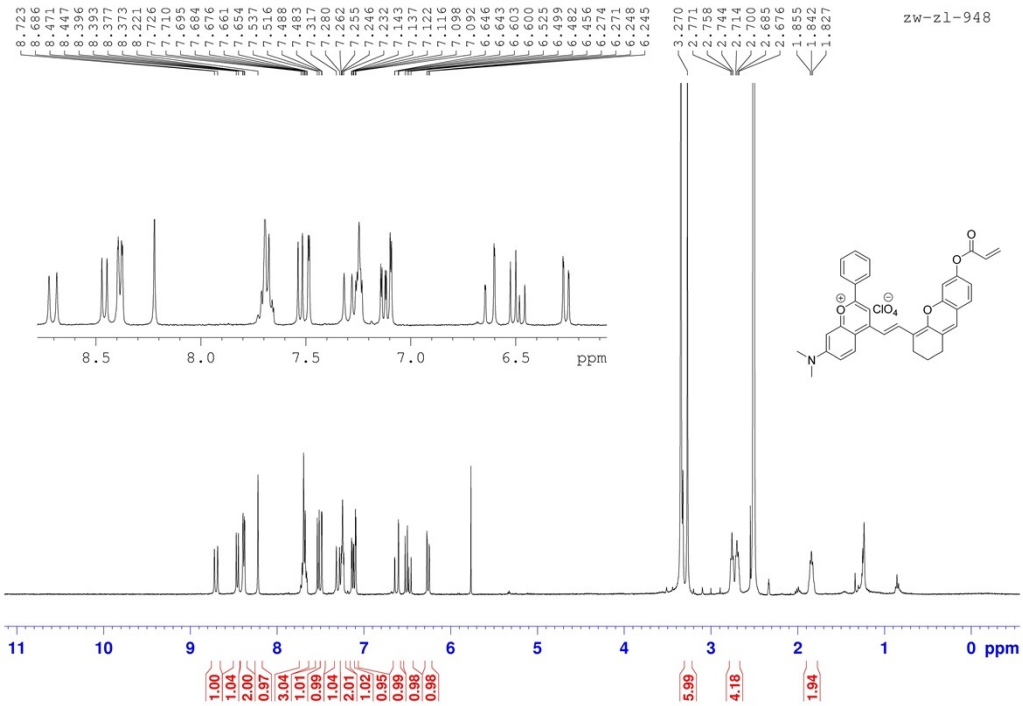

Fig. S37. [1]H NMR spectrum of FC-Cys in DMSO-d_6

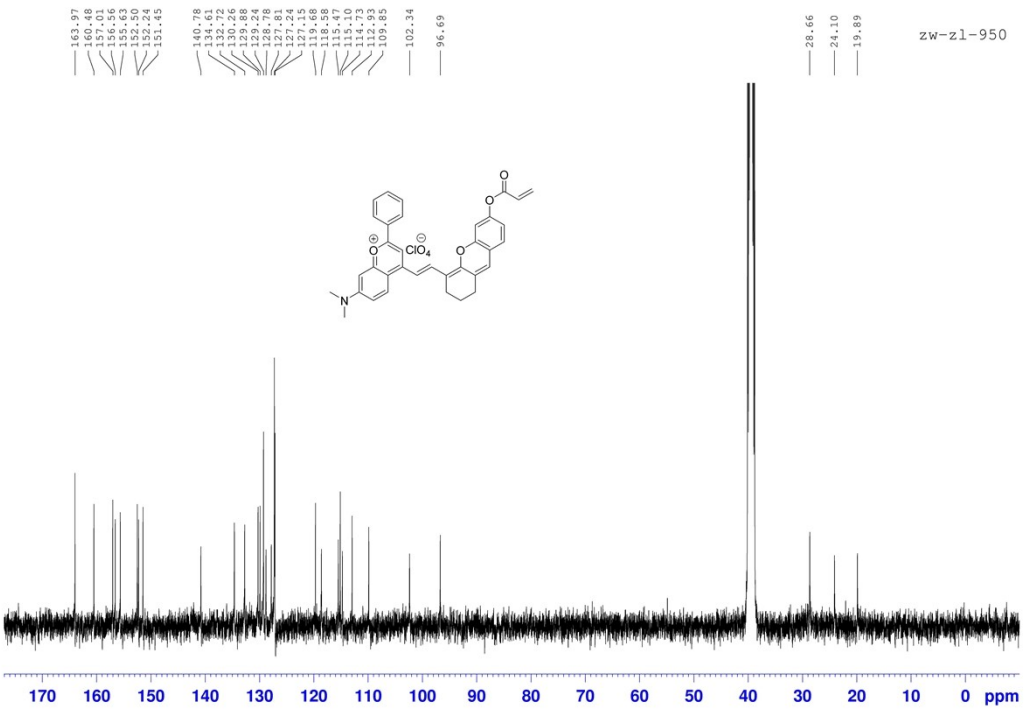

Fig. S38. [13]C NMR spectrum of FC-Cys in DMSO-d_6

Elemental Composition Report **Page 1**

Single Mass Analysis
Tolerance = 5.0 mDa / DBE: min = -1.5, max = 50.0
Element prediction: Off
Number of isotope peaks used for i-FIT = 3

Monoisotopic Mass, Even Electron Ions
4 formula(e) evaluated with 1 results within limits (up to 50 best isotopic matches for each mass)
Elements Used:
C: 0-35 H: 0-30 N: 0-1 O: 0-4
WH-ZHU
ZW-ZL-09263 82 (0.933) Cm (82:83)

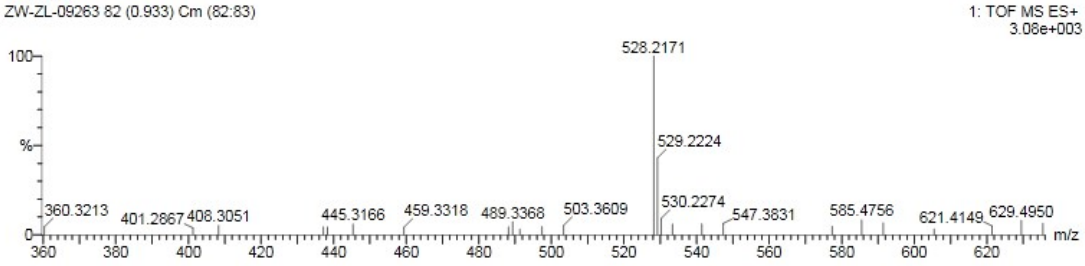

Minimum:				-1.5			
Maximum:		5.0	10.0	50.0			
Mass	Calc. Mass	mDa	PPM	DBE	i-FIT	i-FIT (Norm)	Formula
528.2171	528.2175	-0.4	-0.8	21.5	9.9	0.0	C35 H30 N O4

Fig. S39. HRMS spectrum of FC-Cys.